Light-controlled lyotropic liquid crystallinity of polyaspartates

Max Hirschmann and Christina M. Thiele*

Technical University of Darmstadt, Clemens-Schöpf-Institute, Alarich-Weiss-Straße 4, 64287 Darmstadt (Germany)

In nature, proteins like rhodopsin act as transducer for photo-chemical reactions causing biological responses (e.g. enabling vision)[1]. The underlying concept – a photo-induced conformational change of the protein as amplifier of the photo-responsive moiety – can also be adopted by synthetical polymers or foldamers[2] that have the propensity to form ordered secondary structures (e.g. polypeptides)[3,4]. An alternative approach to amplify photo-chemical responses is their incorporation into liquid crystals[5]. With only a few exceptions[6,7], photo-insensitive liquid crystals are doped with dyes[8,9] that favour disorder upon irradiation[10]. In theory, photo-responsive polypeptides[11], capable of forming lyotropic liquid crystals[12], could exploit both amplification approaches but, in practice, their photo-responsivity is hampered by the reduced mobility of polypeptides in concentrated solutions[13]. Here we show that the E/Z photo-isomerisation of an azobenzene containing polyaspartate initiates a helix-coil backbone transition, which reversibly alters the polypeptide solution from anisotropic to isotropic. In contrast to other photo-responsible polymers[14], in which thermal relaxation to the more stable photo-isomer is quite fast, both photo-isomers are thermally stable and interconvertible by visible light in a single solvent. Local irradiation and magnetic fields lead to spatial resolution and unidirectional architectures of the liquid crystal, respectively. Our results demonstrate that photo-isomerisation on a molecular level is amplified in three stages via intra- and intermolecular interactions to yield a unidirectional, chiral liquid crystal. We believe, the morphological changes of the liquid crystal induced by light will facilitate a multitude of applications, like photo-alignment[15] or the photo-control of solution viscosity[14] and anisotropic

diffusion[16]. When incorporated into layer-by-layer architectures the polymer could find application in biomedicine[17] and the spatial and temporal resolution could be exploited in nano-technology[18].

Poly-[4-(2,6-difluorophenyl)-azo-3,5-difluorobenzyl]-L-aspartate (P*p*FABLA, **1**) was targeted, because polyaspartates in general have the propensity to form rigid secondary structures that are sensitive to side-chain, solvent or temperature variations[11]. Additionally, certain copolyaspartates with high amounts of *p*-phenylazobenzyl-L-aspartate show a light-induced helix-coil transition in 1,2-dichloroethane[19] but the corresponding homopolyaspartate proved insoluble in this solvent[20]. If these polymers were soluble in higher concentrations, their helical conformation would posses the necessary shape anisotropy to form lyotropic liquid crystalline solutions. From our previous investigations on poly-β-benzyl-L-aspartate (PBLA)[21], we know that polyaspartate solubility can crucially depend on the polymer weight and, thus, we believed that solubility issues can be addressed similarly by utilisation of a controlled polymerisation protocol. To overcome the thermal instability of light-induced conformational changes of the polyaspartates mentioned[22], we chose stable $(o\text{-F})_4$-azobenzene[23] instead of the unsubstituted azobenzene. For $(o\text{-F})_4$-azobenzene, Hecht has shown a thermal half-life of 700 d at 25 °C in acetonitrile and a 42 nm separation of the n-π* absorption bands of the two photo-isomers. If the increased separation and bathochromic shift of the n-π* absorption and its reduced extinction coefficient (by one order of magnitude compared to the π-π* absorption band) are transferable to the polymer, the usage of a low-intensity visible light source would allow access to both states with high photo-conversions. Furthermore, this will improve the penetration depth while reducing the photo-induced degradation in future applications[24] of the polymer.

P*p*FABLA (**1**) was synthesised starting from 3,5-difluorobenzaldehyde (**2**) and 2,6-difluoroaniline (**3**) (Extended Data Figure 1). Prior to their coupling[25], the former was reduced to 3,5-difluorotoluene (**4**) and lithiated using *n*-butyllithium while the latter was converted to its diazonium salt (**5**). 4-(2,6-Difluorophenyl)-azo-3,5-difluorotoluene (**6**) was brominated to yield 4-(2,6-difluorophenyl)-azo-3,5-difluorobenzyl bromide (**7**) and further esterified with copper-protected[26] L-aspartic acid (**8**). Conversion

50 of β-aspartate **9** with phosgene[27] to its N-carboxyanhydride **10**, acting as monomer in the subsequent

51 polymerisation[28], yielded P*p*FABLA (**1**).

Switching the secondary structure

53 Investigation of the photo-isomerisation of the azobenzene moieties of P*p*FABLA (**1**) and determination

54 of the optimum wavelengths for selective interconversion of the two isomers are accomplished by

55 acquisition of absorbance spectra (Figure 1, panel a and b). A sample of P*p*FABLA (**1**) in 1,1,2,2-

56 tetrachloroethane (TCE) solution was irradiated with light-emitting diodes (LEDs) with violet light

57 (400 nm, leading to E-**1**) and green light (525 nm, leading to Z-**1**) and the spectra with the highest photo-

58 conversion achieved are displayed (93 % E after violet light irradiation and 95 % Z after green light

59 irradiation). Due to the absence of thermal relaxation after switching of the LED (c.f. next section) the

60 isomer ratio remains the same as in the photostationary state (pss). Thus, it is referred to as pss-E-**1** and

61 pss-Z-**1**, respectively. The azobenzene n-π* absorbance of pss-E-**1** (450 nm) exhibits a bathochromic shift

62 and is separated from pss-Z-**1** (420 nm) by 30 nm. Consequently, excitation of the E-isomer with green

63 light (525 nm) seems ideal, as the optical density is low (enabling excitation of more concentrated

64 polymer solutions as well) and the Z-isomer only weakly absorbs at 525 nm. The azobenzene π-π*

65 absorbance is also different for pss-E-**1** and pss-Z-**1** and, in general, is increased by one order of

66 magnitude compared to the azobenzene n-π* absorbance. This higher optical density (below 380 nm)

67 might impede homogeneous excitation. Thus, violet light (400 nm, n-π* transition) was chosen for

68 efficient excitation of the Z-isomer. The successful excitation and reversible interconversion of E-**1** and

69 Z-**1** in dilute isotropic solution is proven via UV-vis spectra (Figure 1, panel b).
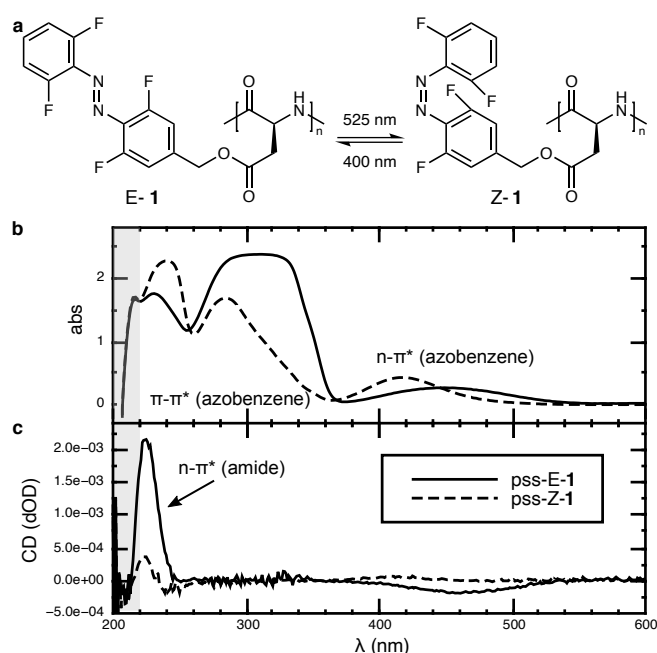
Figure 1. **Photochromism. a**, Reversible photo-isomerisation of P*p*FABLA (**1**), induced by green (525 nm) and violet (400 nm) light, respectively. **b**, UV-vis spectra of both pss (pss-E-**1**, solid line and pss-Z-**1**, dashed line) demonstrate a bathochromic shift of the azobenzene n-π* absorbance (> 380 nm) for E-**1** compared to Z-**1**. **c**, CD spectra reveal a left-handed helical secondary structure of pss-E-**1** (solid line, positive CD of the backbone amide n-π* absorbance, 222 nm) and a random-coil secondary structure of pss-Z-**1** (dashed line, reduced and dispersion-like backbone amide CD). The presence of a small negative CD observed for the pss-E-**1** azobenzene n-π* absorbance (450 nm) suggests a low degree of chiral perturbation of the side-chain by the helical backbone.

70   Simultaneous acquisition of circular dichroism (CD) spectra is used to shed light on the secondary

71   structure of the peptide backbone of pss-E-**1** and pss-Z-**1** (Figure 1, panel c). CD is the different

72   absorbance of oppositely circularly polarised light by chirally perturbed chromophores (CD ≠ 0), while

73   achiral chromophores do not give rise to absorption differences (CD = 0). For pss-E-**1**, a positive CD is

74   observed at 222 nm (amide n-π* absorbance, polypeptide backbone). The sign, intensity, wavelength of

75   maximum CD and shape is characteristic for a periodically ordered, left-handed helical secondary

76   structure of L-configured polyaspartates[19] and, thus, proves that this secondary structure is adopted by pss-

77   E-**1**. A small CD is also observed for the pss-E-**1** azobenzene n-π* absorbance, which indicates a chiral

78   perturbation of the per se achiral side-chain by the left-handed helical backbone. For pss-Z-**1**, the intensity

79   of the CD signature below 250 nm is significantly reduced as compared to pss-E-**1** and has a dispersion-

80   like shape. We believe this reduction in CD is a consequence of a breakdown of the ordered secondary

81   structure of P*p*FABLA (**1**). In principle either a random-coil conformation or a helical secondary structure

4

82 without a predominant handedness (similar amounts of (interconverting) left- and right-handed helices) of

83 pss-Z-**1** would result in a reduction of CD as compared to pss-E-**1**. But the latter could be excluded in this

84 case, because a different spectral pattern would be expected[29]. Thus, we claim that pss-Z-**1** forms a

85 random-coil *induced by* the photo-isomerisation of the azobenzene side-chain.

86 However, the different CD of pss-E-**1** and pss-Z-**1** could also be due to a change in absorption of both

87 photo-isomers in the side-chain (E- *vs.* Z-azobenzene) without a change of the secondary structure. To

88 rule out this *direct* consequence of the photo-isomerisation on the CD observed, a statistical copolymer

89 (P*p*FABLA-*co*-PBLA, **11**) of 75 %(n/n) P*p*FABLA (**1**) and 25 %(n/n) PBLA was synthesised and

90 investigated in the same manner (Extended Data Figure 2). Left-handed helical PBLA has no

91 photochromic moieties and, thus, is chosen with the intention to preserve the left-handed helical

92 polypeptide secondary structure favoured by the E-isomer when converting azobenzenes in P*p*FABLA

93 residues to the Z-isomer. UV-vis and CD spectra of both pss of P*p*FABLA-*co*-PBLA (**11**) show that the

94 photo-isomerisation of its azobenzene moieties still takes place while the secondary structure is preserved

95 in its left-handed helical conformation. Consequently, the different CDs observed for both pss of

96 P*p*FABLA (**1**) are proven to be the result of a change in backbone secondary structure *induced by* the

97 photo-isomerisation of the side-chain.

98 For monitoring the photochromism of P*p*FABLA (**1**), a different analytical method is required, in which

99 the acquisition of data does not interfere with the light used for excitation and is found in *in-situ*

100 irradiation NMR spectroscopy[30–32]. An isotropic solution of P*p*FABLA (**1**) in TCE-d_2 is measured by time-

101 resolved ^{19}F NMR spectroscopy while being irradiated using the same LEDs already used for excitation

102 of the UV-vis samples (Figure 2). When considering only the isolated side-chain, fluorines attached to the

103 same ring of a given isomer are isochronous (identical ^{19}F NMR chemical shift), resulting in a total of

104 four signals expected for mixtures of E-**1** and Z-**1** (inner and outer ring of azobenzene of either E- and Z-

105 isomer). The signal ratio within each isomer is 1:1 and the signal ratio between isomers should yield the

106 ratio of E- and Z-isomer. In the absence of a change in secondary structure as in P*p*FABLA-*co*-PBLA (**11**)

107 quantification of isomers is found to be possible (Extended Data Figure 3). However, for P*p*FABLA (**1**)

108 the side-chain cannot be regarded as isolated from the backbone and different signal sets of the E-isomer

109 moieties are expected for pss-E-**1** and pss-Z-**1.** This complicates quantification of the isomers (signal

110 overlap) and only a rough estimate of E/Z-ratios is possible (Extended Data Figure 4). Nonetheless,

111 irradiation of pss-Z-**1** first with violet light (60 min) and afterwards with green light (120 min) leads to

112 pss-E-**1** and back to pss-Z-**1**, respectively. Compared to the UV-vis samples and despite using the same

113 LEDs, the equilibration time needed is increased by two orders of magnitude, because light intensity is

114 lost inside the waveguide. Furthermore, the NMR samples were more concentrated (increased optical

115 density) and thicker (increased path lengths). After turning off the light, the Z-isomer proves thermally

116 stable at 20 °C over the course of one day. Thus, the outstanding thermal stability is highlighted as

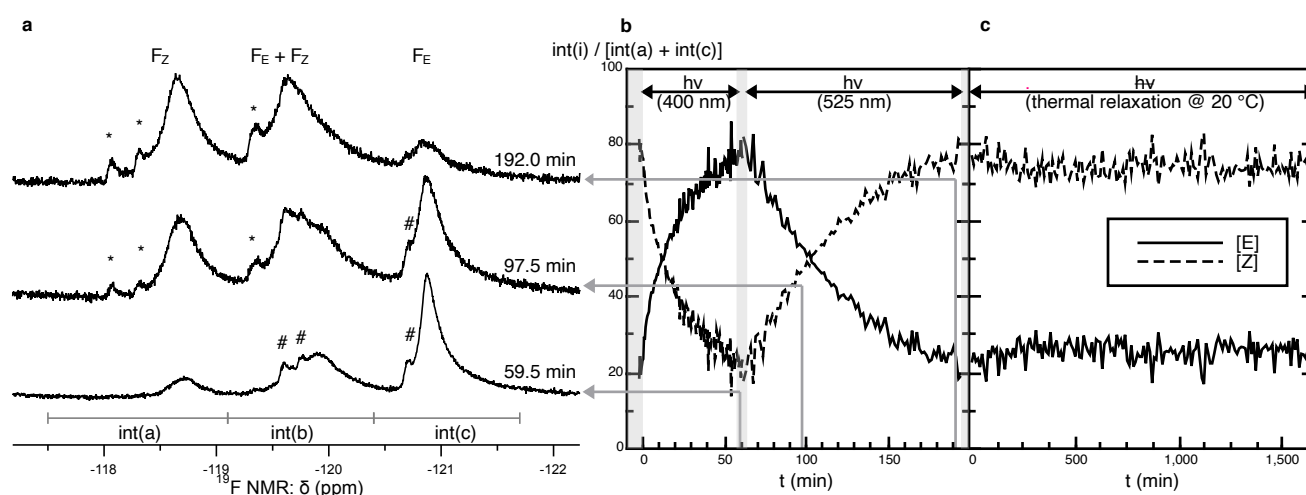117 compared to previously mentioned azobenzene-containing polyaspartates, which fade within minutes[22].

Figure 2. **Monitoring photochromism. a**, ^{19}F NMR spectra of P*p*FABLA (**1**), acquired at 59.5, 97.5 and 192.0 min (pss-E-**1**, mixed state and pss-Z-**1**, respectively). Additional signals for high ratios of either E- or Z-isomers observed (marked with # and *, respectively) complicate quantification of the spectra. Thus, integral ratios should be viewed with caution and should serve only as rough estimate of the E/Z-ratio. **b**, Fraction of integrals a (Z-isomer, dashed line) and c (E-isomer, solid line) plotted *vs.* time obtained by *in-situ* irradiation NMR experiments with violet (400 nm) and green (525 nm) light for 60 and 120 min, respectively. **c**, Similar plot obtained in the absence of irradiation at 20 °C demonstrating the thermal stability of Z-**1**.

Switching between lyotropic liquid crystal and isotropic liquid

119 So far investigations were made in isotropic, dilute polymer solutions. For further amplification of the

120 photo-isomerisation (beyond the induction of a change of secondary structure) 20 %(w/w) solutions of

121 P*p*FABLA (**1**) in TCE-*d₂* were prepared. This concentration should enable the formation of a lyotropic

6

122 liquid crystal for the rod-like pss-E-**1**. Although detection of the E-isomer content of this sample was not

123 possible due to its high optical density (impeding acquisition of UV-vis spectra) and broad ^{19}F NMR

124 signals (no quantification possible), the sample was irradiated with two violet LEDs for one week and

125 afterwards is assumed to consist majorly of the E-isomer (for consistency also referred to as pss-E-**1**). The

126 sample appeared bright between crossed polarisers, which is characteristic for an anisotropic solution due

127 to its birefringence. Irradiation of the sample for two days with a green LED resulted in the pss-Z-**1**,

128 which appeared dark between crossed polarisers (isotropic solution, no birefringence). To our delight, the

129 birefringence was restored by irradiation with two violet LEDs for another week as confirmed by its

130 bright appearance between crossed polarisers. This indicates that for a 20 %(w/w) P*p*FABLA (**1**) solution,

131 the lyotropic liquid crystallinity is switched on and off by visible light.

132 Additionally to visual observations of birefringence the sample was introduced into the magnetic field of

133 an NMR spectrometer and ^{2}H NMR spectra of the solvent were measured[33] (Extended Data Figure 5). In

134 isotropic solution a singlet is expected for TCE-d_2 as both deuterium nuclei are isochronous, which is

135 observed for pss-Z-**1**. For anisotropic solutions without uniform macroscopic orientation (randomly

136 distributed subdomains) the quadrupolar splitting (averaged to zero in isotropic solution) results in a Pake

137 doublet[34] – a broad doublet with two horns and feet. If the anisotropic solution is oriented unidirectionally,

138 however, a regular, sharp doublet is expected for a homogenous sample instead of the Pake doublet[35]. The

139 latter sharp doublet is observed for pss-E-**1**, not only verifying the sample's anisotropy and its restoration

140 after being fully isotropic (pss-Z-**1**) but also proving unidirectionality of the lyotropic liquid crystal

141 induced by the magnetic field.

142 Another benefit of light as stimulus is based on its spatial controllability[36], which would enable further

143 photo-control. The aforementioned anisotropic NMR sample (pss-E-**1**) was only partially irradiated with

144 the green LED for two days. The sample's lower, irradiated part was thus converted to pss-Z-**1** while the

145 upper, non-irradiated part remained in pss-E-**1** (Figure 3). A distinct phase boundary is observed both on

146 direct sight and between crossed polarisers revealing the successful spatial resolution of isotropic solution

147 and lyotropic liquid crystal. The sample turns out to be stable for several days. Additionally, the formation

148 of a unidirectional lyotropic liquid crystal (upper part) and of an isotropic solution (lower part) was

149 verified by ^{2}H z-image NMR spectroscopy[37], in which spatially resolved spectra show the characteristic

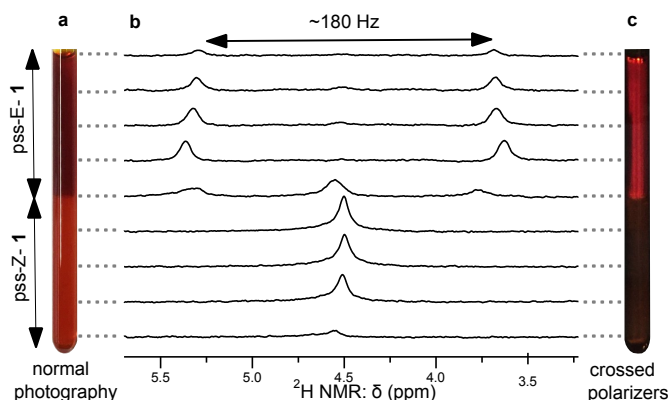150 solvent doublet and singlet, respectively.

151

Figure 3. **Spatial resolution and unidirectionality.** A sample of 20 %(w/w) PpFABLA (**1**) dissolved in TCE-d_2 inside a 3 mm NMR tube. The previously homogeneous pss-E-**1** sample has been irradiated locally with green light resulting in the lower part to be in pss-Z-**1** while the upper part remains in pss-E-**1**. **a**, Photograph of the sample, the lower part is orange and the upper part is red. **b**, ^{2}H z-image NMR spectra of the solvent: For the lower and upper part, a singlet and a sharp doublet are observed, respectively, indicating isotropic and anisotropic phases. **c**, Photograph of the sample between crossed polarisers. The anisotropic upper part appears bright (birefringence), whereas the lower part is dark (isotropic).

152 **Photo-switchable alignment**

153 So far the polypeptide solution is proven to be switched reversibly from an anisotropic lyotropic liquid

154 crystal to an isotropic state. In a next step, we investigate the influence of this change on intermolecular

155 interactions between probe molecules and the polymer. As the lyotropic liquid crystal is inherently chiral

156 due to the one-handed helical backbone of the polypeptide, its enantiomer differentiation capabilities[38,39]

157 were simultaneously tested. Therefore, either (+)- or (–)-IPC additionally dissolved in the NMR sample as

158 probe molecules were investigated (Figure 4, panel a). Usually enantiomers are not distinguishable in

159 conventional NMR spectroscopy and show identical signals. However, dissolution of enantiomers into a

160 homochiral lyotropic liquid crystal enables intermolecular, diastereomorphous interactions ((+)-IPC with

161 L-polymer **1** *vs.* (–)-IPC with L-polymer **1**) leading to different induced mean orientations of the

162 enantiomers with respect to the NMR spectrometer's magnetic field. This can lead to different anisotropic

163 NMR observables like dipolar couplings (D). In anisotropic solution, the dipolar coupling adds up onto

164 the scalar coupling (J, directly measurable in isotropic solution) resulting in the total coupling (T) (Figure

165 4, panel b). In the absence of anisotropy (pss-Z-**1**) no dipolar couplings were measured, which is expected

166 due to their averaging to zero in isotropic solution (Figure 4, panel c). For pss-E-**1** dipolar couplings of

167 both enantiomers were measured. Interestingly, these are different for certain coupling partners (e.g. C2-

168 H2), which proves a successful and chiral alignment transfer of the lyotropic liquid crystal onto the

169 dissolved probe molecules. The enantiomer differentiation capabilities can further be quantified by using

170 the β_{5D}-angle[40] to be 17.5° (with 0° and 90° corresponding to no and maximum differentiation,
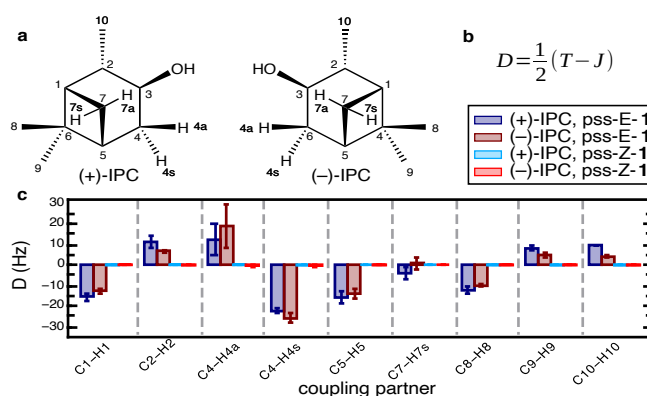
171 respectively).

Figure 4. **Photo-controlled alignment. a**, Structures of (+)- and (−)-IPC used as probe molecules (introduced into a 20 %(w/w) P*p*FABLA (**1**) solution in TCE-d_2). **b**, Equation used for calculation of the dipolar coupling (D) by measurement of the total (T, sample: IPC + P*p*FABLA (**1**) + TCE-d_2) and scalar (J, sample: IPC + TCE-d_2) coupling. **c**, Dipolar couplings (D) of (+)- and (−)-IPC (blue and red, respectively) in either pss-E-**1** (dark coloured item) or pss-Z-**1** (bright coloured item) containing samples. For pss-Z-**1**, D is zero, which is expected for an isotropic solution. Differences of D between (+)- and (−)-IPC (e.g. for C2-H2) result from the enantiomer differentiation capabilities of the liquid crystal. The coupling of C3-H3 and C7-H7a could not be extracted.

172 For the measurement of dipolar couplings, P*p*FABLA (**1**) thus proves directly useful as it allows for

173 acquisition of the scalar and total coupling using only one sample, which could further be measured

174 simultaneously by exploitation of spatial resolution (isotropic and anisotropic part of the sample,

175 respectively) and acquisition of spatially resolved[41] NMR spectra (Extended Data Figure 6).

176 Additionally, P*p*FABLA-*co*-PBLA (**11**) was tested for its enantiomer differentiation capabilities likewise.

177 Dipolar coupling sets of (+)- and (–)-IPC, respectively, obtained for pss-E-**11** and pss-Z-**11** exhibit a small

178 but noticeable difference. Thus, the preserved secondary structure but different photo-isomers of the side-

179 chains of P*p*FABLA-*co*-PBLA (**11**) upon irradiation affects the alignment induced onto IPC and their

180 enantiomeric differentiation.

181 **Conclusions**

182 In summary, the photo-isomerisation of the (*o*-F)$_4$-azobenzene moieties of P*p*FABLA (**1**) have been

183 shown to be amplified in three stages via the change of the polypeptide secondary structure, the formation

184 of a lyotropic liquid crystal and its unidirectional orientation by a magnetic field. The helix-coil transition

185 of the polypeptide by itself is remarkable, as it is thermally stable and can be selectively altered with

186 violet (400 nm) and green (525 nm) light, respectively, even in highly viscous solutions. Such drastic

187 secondary structure changes can be exploited in the future in the fields of e.g. layer-by-layer polymer

188 architectures in biomedical applications[17]. Reversible control of the state of matter (lyotropic liquid

189 crystal *vs.* isotropic solution) and its directionality enable regulation of solution viscosity[14] and anisotropic

190 diffusion[16]. Furthermore, macroscopic lyotropic liquid crystal and isotropic domains are obtainable by

191 exploitation of spatial controllability by light. This represents a fourth stage of photo-control and might

192 enable e.g. photo alignment[15] and its usage in nano technology[18] in the future. The lyotropic liquid crystal

193 has further been shown to transfer its chirality onto probe molecules dissolved therein. This can be

194 regarded as light-induced enantiomer differentiation. Future work aims at lowering the optical density of

195 the system by development of new azobenzene-containing (co)-polyaspartates and, thus, reducing the

196 total amount of azobenzene-moieties necessary to induce a change in secondary structure.

197 References

198 1.   Hofmann, K. P. *et al.* A G protein-coupled receptor at work: the rhodopsin model. *Trends*

199 *Biochem. Sci.* **34**, 540–552 (2009).

200   2.   Yu, Z. & Hecht, S. Remote control over folding by light. *Chem. Commun.* **52**, 6639–6653 (2016).

201   3.   Ciardelli, F., Bronco, S., Pieroni, O. & Pucci, A. Photoswitchable polypeptides. *Mol. Switch.* **1**,

202   321–360 (2011).

203   4.   Le Bailly, B. A. F. & Clayden, J. Dynamic foldamer chemistry. *Chem. Commun.* **52**, 4852–4863

204   (2016).

205   5.   Bisoyi, H. K. & Li, Q. Light-Driven Liquid Crystalline Materials: From Photo-Induced Phase

206   Transitions and Property Modulations to Applications. *Chem. Rev.* **116**, 15089–15166 (2016).

207   6.   Kosa, T. *et al.* Light-induced liquid crystallinity. *Nature* **485**, 347–349 (2012).

208   7.   Peng, S., Guo, Q., Hughes, T. C. & Hartley, P. G. Reversible Photorheological Lyotropic Liquid

209   Crystals. *Langmuir* **30**, 866–872 (2014).

210   8.   Katsonis, N., Lacaze, E. & Ferrarini, A. Controlling chirality with helix inversion in cholesteric

211   liquid crystals. *J. Mater. Chem.* **22**, 7088–7097 (2012).

212   9.   Bisoyi, H. K. & Li, Q. Light-directed dynamic chirality inversion in functional self-organized

213   helical superstructures. *Angew. Chem. Int. Ed.* **55**, 2994–3010 (2016).

214   10.   Ichimura, K. Photoalignment of Liquid-Crystal Systems. *Chem. Rev.* **100**, 1847–1874 (2000).

215   11.   De Zotti, M. *et al.* Handedness preference and switching of peptide helices. Part I: Helices based

216   on protein amino acids. *J. Pept. Sci.* **20**, 307–322 (2014).

217   12.   Robinson, C. LIQUID-CRYSTALLINE STRUCTURES IN SOLUTIONS OF A POLYPEPTIDE.

218   *Trans. Faraday Soc.* **52**, 571–592 (1956).

219   13.   Ueno, A., Morikawa, Y., Anzai, J. & Osa, T. Conformational versatility of polyaspartates with (p-

220   phenylazo)phenethyl side chains in solid films. *Makromol Chem Rapid Commun* **5**, 639–642 (1984).

221   14.   Szymański, W., Beierle, J. M., Kistemaker, H. A. V., Velema, W. A. & Feringa, B. L. Reversible

222   Photocontrol of Biological Systems by the Incorporation of Molecular Photoswitches. *Chem. Rev.* **113**,

223   6114–6178 (2013).

224   15.   Aizawa, M., Barrett, C. J. & Shishido, A. Photo-Control of Molecular Alignment for Photonic and

225   Mechanical Applications. *Mol. Technol. Vol. 1 Energy Innov.* (2018).

226   16.   Yin, Y. *et al.* Diffusional behavior of polypeptides in the isotropic, biphasic, and liquid crystalline

227   phases as studied by the pulse field-gradient Spin−Echo 1H NMR method. *Macromolecules* **35**, 5910–

228   5915 (2002).

229   17.   Akiba, U., Minaki, D. & Anzai, J. Photosensitive layer-by-layer assemblies containing azobenzene

230   groups: Synthesis and biomedical applications. *Polymers* **9**, 553 (2017).

231   18.   Wang, L. & Li, Q. Photochromism into nanosystems: towards lighting up the future nanoworld.

232   *Chem. Soc. Rev.* **47**, 1044–1097 (2018).

233   19.   Ueno, A., Takahashi, K., Anzai, J. & Osa, T. Reversible conformational changes induced by light

234   in copolymers of two phenylazo-substituted aspartic acids. *Makromol. Chem.* **182**, 693–695 (1981).

235   20.   Ueno, A., Anzai, J., Osa, T. & Kadoma, Y. Light-induced conformational changes of polypeptides.

236   Random copolymers of γ-Benzyl-L-glutamate with m- and p-Phenylazobenzyl-L-aspartates. *Bull. Chem.*

237   *Soc. Jpn.* **50**, 2995–2999 (1977).

238   21.   Hirschmann, M., Schwab, M. & Thiele, C. M. Molecular weights: The key for lyotropic liquid

239   crystalline phases of poly-β-benzyl-l-aspartate. *Macromolecules* **52**, 6025–6034 (2019).

240   22.   Ueno, A., Anzai, J. & Osa, T. Thermal isomerization of azoaromatic residues in the side chain of

241   polypeptides. *J Polym Sci Polym Lett Ed* **17**, 149–154 (1979).

242   23.   Bléger, D., Schwarz, J., Brouwer, A. M. & Hecht, S. o-Fluoroazobenzenes as readily synthesized

243   photoswitches offering nearly quantitative two-way isomerization with visible light. *J. Am. Chem. Soc.*

244   **134**, 20597–20600 (2012).

245   24.   Boase, N. R. B. Shining a Light on Bioorthogonal Photochemistry for Polymer Science.

246   *Macromol. Rapid Commun.* **41**, 2000305 (2020).

247   25.   Hansen, M. J., Lerch, M. M., Szymanski, W. & Feringa, B. L. Direct and versatile synthesis of

248   red-shifted azobenzenes. *Angew. Chem. Int. Ed.* **55**, 13514–13518 (2016).

249   26.   Heeswijk, W. A. R. van, Eenink, M. J. D. & Feijen, J. An improved method for the preparation of

250   gamma-Esters of glutamic acid and beta-Esters of aspartic acid. *Synthesis* **9**, 744–747 (1982).

251   27.   Fuller, W. D., Verlander, M. S. & Goodman, M. A procedure for the facile synthesis of amino-acid

252   N-Carboxyanhydrides. *Biopolymers* **15**, 1969–1971 (1976).

253   28.   Zhao, W., Gnanou, Y. & Hadjichristidis, N. Organocatalysis by hydrogen-bonding: a new

254   approach to controlled/living polymerization of α-amino acid N-carboxyanhydrides. *Polym. Chem.* **6**,

255   6193–6201 (2015).

256   29.   Ueno, A., Takahashi, K., Anzai, J. & Osa, T. Photocontrol of polypeptide helix sense by cis-trans

257   isomerism of side-chain azobenzene moieties. *J. Am. Chem. Soc.* **103**, 6410–6415 (1981).

258   30.   Feldmeier, C., Bartling, H., Riedle, E. & Gschwind, R. M. LED based NMR illumination device

259   for mechanistic studies on photochemical reactions – Versatile and simple, yet surprisingly powerful. *J.*

260   *Magn. Reson.* **232**, 39–44 (2013).

261   31.   Kind, J., Kaltschnee, L., Leyendecker, M. & Thiele, C. M. Distinction of trans–cis photoisomers

262   with comparable optical properties in multiple-state photochromic systems – examining a molecule with

263   three azobenzenes via in situ irradiation NMR spectroscopy. *Chem. Commun.* **52**, 12506–12509 (2016).

264 32.   Nitschke, P., Lokesh, N. & Gschwind, R. M. Combination of illumination and high resolution

265 NMR spectroscopy: Key features and practical aspects, photochemical applications, and new concepts.

266 *Prog. Nucl. Magn. Reson. Spectrosc.* **114–115**, 86–134 (2019).

267 33.   Thiele, C. M. Use of RDCs in rigid organic compounds and some practical considerations

268 concerning alignment media. *Concepts Magn. Reson. Part A* **30A**, 65–80 (2007).

269 34.   Pake, G. E. Nuclear Resonance Absorption in Hydrated Crystals: Fine Structure of the Proton

270 Line. *J. Chem. Phys.* **16**, 327–336 (1948).

271 35.   Jeziorowski, S. & Thiele, C. M. Poly-γ-p-biphenylmethyl-glutamate as enantiodifferentiating

272 alignment medium for NMR spectroscopy with temperature-tunable properties. *Chem. – Eur. J.* **24**,

273 15631–15637 (2018).

274 36.   Albert, L. & Vázquez, O. Photoswitchable peptides for spatiotemporal control of biological

275 functions. *Chem. Commun.* **55**, 10192–10213 (2019).

276 37.   Trigo-Mouriño, P., Merle, C., Koos, M. R. M., Luy, B. & Gil, R. R. Probing spatial distribution of

277 alignment by deuterium NMR imaging. *Chem. – Eur. J.* **19**, 7013–7019 (2013).

278 38.   Lesot, P., Gounelle, Y., Merlet, D., Loewenstein, A. & Courtieu, J. Measurement and analysis of

279 the molecular ordering tensors of two enantiomers oriented in a polypeptide liquid crystalline system. *J.*

280 *Phys. Chem.* **99**, 14871–14875 (1995).

281 39.   Lesot, P. *et al.* Multinuclear NMR in polypeptide liquid crystals: Three fertile decades of

282 methodological developments and analytical challenges. *Prog. Nucl. Magn. Reson. Spectrosc.* **116**, 85–

283 154 (2020).

284 40.   Kramer, F., Deshmukh, M. V., Kessler, H. & Glaser, S. J. Residual dipolar coupling constants: An

285 elementary derivation of key equations. *Concepts Magn. Reson. Part A* **21A**, 10–21 (2004).

286   41.   Reller, M., Wesp, S., Koos, M. R. M., Reggelin, M. & Luy, B. Biphasic liquid crystal and the

287   simultaneous measurement of isotropic and anisotropic parameters by spatially resolved NMR

288   spectroscopy. *Chem. – Eur. J.* **23**, 13351–13359 (2017).

Methods

P*p*FABLA (**1**) and P*p*FABLA-*co*-PBLA (**11**) were synthesised starting from commercially available

sources (Extended Data Figure 1). The detailed synthesis procedures and compound characterisation data

are given in the supporting information. Irradiation of the polymers is performed using green (525 nm

absorption maximum, LUXEON CZ Color Line, part number: L1CU-GRN1000000000) and violet

(400 nm absorption maximum, LUXEON UV U Line, part number: LHUV-0405) LEDs from Lumileds.

The light intensity depends on the measurement setup, is always reduced compared to the radiometric

power of the LEDs and could thus not be used to determine the quantum efficiency of the photo-

conversion.

UV-vis and CD spectroscopy

UV-vis and CD spectra were recorded simultaneously on a JASCO J-1500 spectrometer equipped with a

PTC-510 peltier element (at 20 °C) and a PM-539 detector. Spectra were recorded in a wavelength range

from 600 to 200 nm, with a data interval of 1 nm, a bandwidth of 2 nm, an integration time of 0.5 s and a

scanning speed of 200 nm/min. Polymer solutions (0.076 M, per residue) were prepared by dissolving the

polymer over night in TCE, were placed inside a demountable cuvette[42] with a path length < 10 μm

(necessary to lower the solvent cut-off to ~215 nm, defined by a high tension (HT) voltage > 500 V) and

were irradiated inside the cuvette holder for 5 min with a violet LED prior to the first measurement of a

measurement series (ensuring pss-E of the sample). After each measurement within the series, the sample

was irradiated first with a green LED for a few seconds until no further spectral changes were observed

(pss-Z reached) and after that with a violet LED for a few seconds until the sample is restored in pss-E.

The measurement series thus consist of approx. 10 individual spectra of the polymer in different E/Z-

ratios. Prior to analysis, a background correction was performed by subtraction of signals obtained from

pure TCE. The spectra thus obtained could only be interpreted qualitatively due to the absolute path

length uncertainty for demountable cuvettes[43] that further prevent the calculation of the extinction

313   coefficient (UV-vis) and the molar ellipticity (CD). The whole measurement series for each polymer is

314   given in the supporting information.

315   **_In-situ_ irradiation NMR spectroscopy**

316   ^{19}F NMR spectra were recorded on a Bruker Avance III HD NMR spectrometer (400 MHz proton

317   frequency) equipped with a 5 mm BBFO probe with z-gradient. Polymer solutions (22.3 g/L for

318   P*p*FABLA (**1**) and 10 g/L for P*p*FABLA-*co*-PBLA (**11**)) in TCE-d_2 were prepared and 0.45 mL thereof

319   placed inside a thin-wall 5 mm NMR tube that was closed with a coaxial insert (Wilmad-LabGlass)[30]. A

320   waveguide (0.39 NA TECS-Clad Multimode Optical Fiber from Thorlabs) with roughened tip was

321   inserted enabling irradiation of the sample inside the NMR spectrometer. The receiving end of the

322   waveguide was attached to the LEDs by an SMA connector. Prior to the measurement of ^{19}F NMR spectra

323   series, a pulse length optimisation and a T_1 relaxation time determination were performed. The sample

324   was irradiated with the green LED until no further spectral changes were observed (pss-Z). ^{19}F NMR

325   spectra series were recorded at 20 °C by accumulation of 4 scans with a recovery delay *D1* of 2.5–3.0 s

326   and a time interval between experiments of 30 s and 10 min. The sample was first irradiated with a violet

327   LED (conversion of Z-isomer into E-isomer), followed by irradiation with a green LED (conversion of E-

328   isomer into Z-isomer) and finally irradiation was stopped to investigate thermal relaxation of the Z-

329   isomer. Individual spectra thus obtained were phase and baseline corrected and signal intensities were

330   obtained by integration of 3 spectral regions (integral a: −117.5 to −119.1 ppm, integral b: −119.1 to −

331   120.4 ppm and integral c: −120.4 to −121.7 ppm), which were further used to estimate the E/Z ratio of the

332   polymer. Although acquisition of NMR spectra was assured to be quantitative ($D1 > 5T_1$), the

333   quantification of E/Z ratio was only possible for P*p*FABLA-*co*-PBLA (**11**), presumably due to the drastic

334   conformational changes of P*p*FABLA (**1**) leading to two signal sets for the respective E-isomers

335   (Extended Data Figure 4).

17

Concentrated polymer samples

4 samples were prepared by dissolving either P*p*FABLA (**1**, 20 %(w/w)) or P*p*FABLA-*co*-PBLA (**11**, 16 %(w/w)) together with (+)- and (−)-IPC, respectively in TCE-d_2 directly inside a 3 mm NMR tube (sample composition is given in the supporting information). The NMR samples were frozen, evacuated and sealed by melting the top of the NMR tube using a propane torch. Sample homogeneity was established by centrifuging the sample back and forth while heating the sample in between each centrifugation step. Prior to the first NMR measurements, the samples were irradiated by two violet LEDs (from opposite sides) inside an aluminium box[44] resulting in pss-E. To change the E/Z ratio, the samples were irradiated with a green LED or two violet LEDs either homogeneously or with spatial control (detailed sample history and irradiation times are given in the supporting information). Homogeneously irradiated samples were further centrifuged back and forth again after irradiation to enhance sample homogeneity.

Prior to NMR measurements, the sealed polymer samples were placed inside a 5 mm NMR tube filled additionally with acetone-d_6 to enable locking and shimming. However, the outer 5 mm NMR tube was not tightly sealed and, thus, was prone to take up water (air humidity), which was observed as additional signal of HDO in ^{2}H NMR spectra (^{2}H and ^{19}F NMR spectra of all samples are given in the supporting information).

NMR spectroscopy of concentrated polymer samples

Spectra were recorded on a Bruker Avance III HD NMR spectrometer (700 MHz proton frequency) equipped with a QCI cryo probe with z-gradient. ^{2}H, ^{2}H z-image and ^{19}F z-image NMR spectra were measured to ensure sample homogeneity and to observe the spatial resolution of partially irradiated samples[37].

CLIP-HSQC NMR spectra[45] were measured with an INEPT delay of 145 Hz, a spectral width of 10 (8192 data points, 2 ppm offset) and 35 ppm (512 data points, 32.5 ppm offset) in the direct and indirect dimension, respectively, and accumulated over 4 scans per increment. For partially irradiated samples a

spatially selective version[41] of the CLIP HSQC NMR spectrum was used instead with similar acquisition parameters. To obtain spatial selectivity a slice width of 0.5 cm and a spatial offset of 0.5 and −0.5 cm from the centre of the coil to excite the upper and lower part of the sample, respectively, were used as additional parameters and the number of scans was adjusted to 60. Additionally, F1-coupled HSQC NMR spectra[46] were measured for samples consisting of PpFABLA (**1**) to enhance the total number of couplings extractable for IPC. Acquisition parameters were chosen as follows: INEPT delay of 145 Hz, scaling factor of 8, a spectral width of 10 (1398 data points, 2 ppm offset) and 80 ppm (4096 data points, 45 ppm offset) in the direct and indirect dimension, respectively, and 2 scans. A zero filling of two in both dimensions and a shifted squared sine window function was used for processing of the 2D NMR spectra.

Analysis of dipolar couplings

Total couplings of IPC were extracted from the 2D NMR spectra[47] and used to calculate the dipolar coupling following the $T=2D+J$ convention by using the scalar couplings of IPC[21]. Proton carbon dipolar couplings of methyl groups were further converted into carbon carbon dipolar couplings of the methyl group and the adjacent carbon[48]. For conversion gyromagnetic ratios of $6.728 \cdot 10^7$ rad/(T s) and $26.752 \cdot 10^7$ rad/(T s) for ^{13}C and ^{1}H, respectively, and bond lengths of 150.7 and 109.1 pm for carbon carbon and carbon proton bonds, respectively, were used. The dipolar couplings together with a structural model of IPC[21] were used as input for the program RDC@hotFCHT[49,50] to calculate the alignment tensor and alignment values derived thereof (couplings extracted and alignment values calculated are given in the supplementary information).

Methods References

42. Hirschmann, M., Merten, C. & Thiele, C. M. Circular Dichroism of Lyotropic Liquid Crystalline Polyaspartate Solution Reveals Temperature-Induced Reversal of Cholesteric Sense. submitted to *Soft Matter*.

43. Miles, A. J. & Wallace, B. A. Circular dichroism spectroscopy of membrane proteins. *Chem. Soc. Rev.* **45**, 4859–4872 (2016).

44. Niedek, D. *et al.* In Situ Switching of Site-Selectivity with Light in the Acetylation of Sugars with Azopeptide Catalysts. *J. Org. Chem.* **85**, 1835–1846 (2020).

45. Enthart, A., Freudenberger, J. C., Furrer, J., Kessler, H. & Luy, B. The CLIP/CLAP-HSQC: Pure absorptive spectra for the measurement of one-bond couplings. *J. Magn. Reson.* **192**, 314–322 (2008).

46. Thiele, C. M. & Bermel, W. Speeding up the measurement of one-bond scalar (1J) and residual dipolar couplings (1D) by using non-uniform sampling (NUS). *J. Magn. Reson.* **216**, 134–143 (2012).

47. Kummerlöwe, G., Schmitt, S. & Luy, B. Cross-fitting of residual dipolar couplings. *Open Spectrosc. J.* **4**, 16–27 (2010).

48. Verdier, L., Sakhaii, P., Zweckstetter, M. & Griesinger, C. Measurement of long range H,C couplings in natural products in orienting media: a tool for structure elucidation of natural products. *J. Magn. Reson.* **163**, 353–359 (2003).

49. Berger, R., Fischer, C. & Klessinger, M. Calculation of the Vibronic Fine Structure in Electronic Spectra at Higher Temperatures. 1. Benzene and Pyrazine. *J. Phys. Chem. A* **102**, 7157–7167 (1998).

50. Schmidts, V. Entwicklung einer Auswertungssoftware zur Anwendung residualer dipolarer Kopplungen in der organischen Strukturaufklärung. (PhD Thesis, TU Darmstadt, 2013).

51. Bak, M., Rasmussen, J. T. & Nielsen, N. Chr. SIMPSON: A general simulation program for solid-state NMR spectroscopy. *J. Mag. Reson.* **147**, 296–330 (2000).

Acknowledgements

Author Contributions

Both authors conceived the project and discussed the results. Syntheses, characterisation of compounds, sample preparation and acquisition of UV-vis, CD and NMR spectra was done by M.H. The manuscript was written by M.H. with revisions provided by C.M.T. The project was supervised by C.M.T.
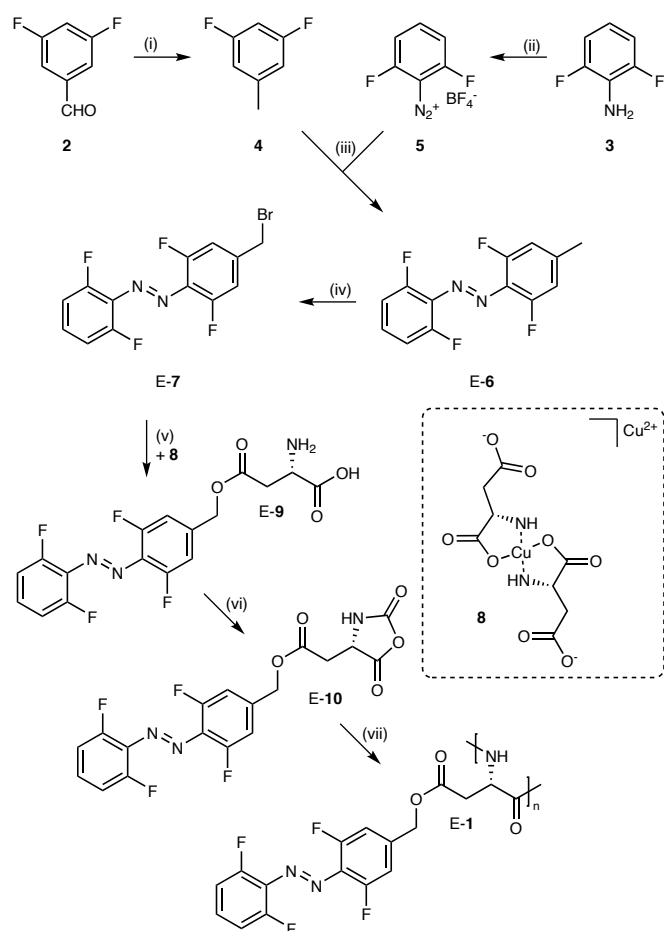
Competing Interest Declaration
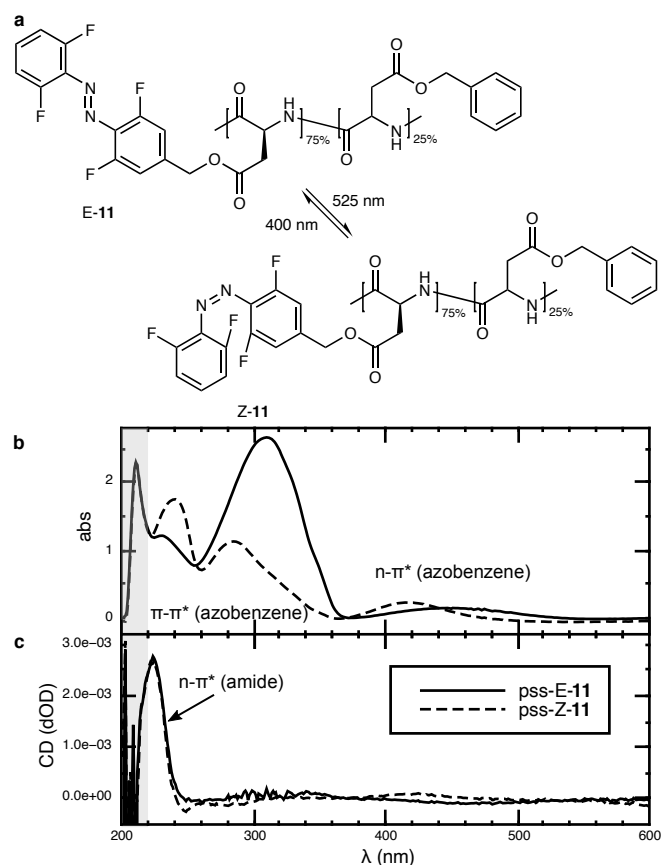
The authors declare no competing interest.

Additional Information

supplementary information is available for this article

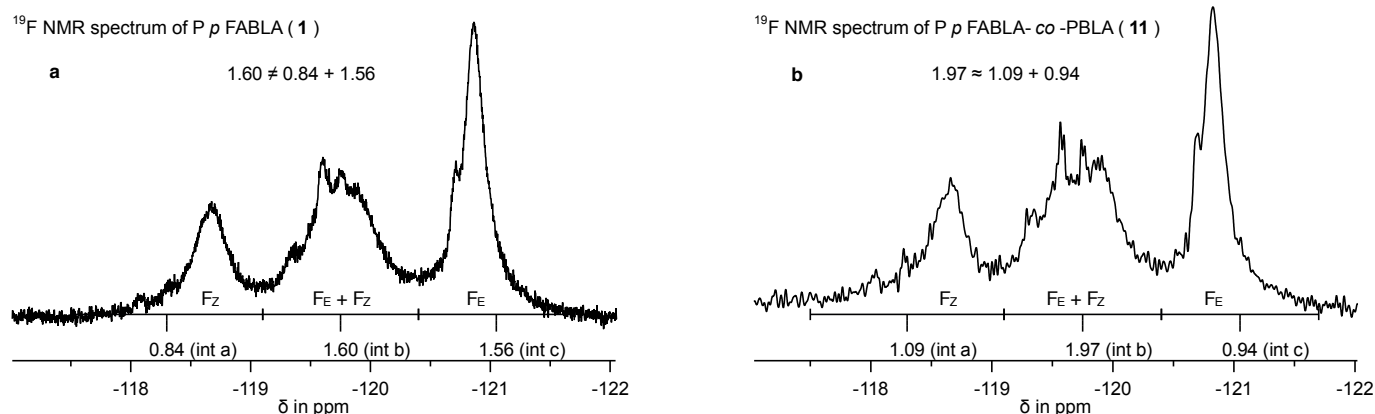correspondence should be addressed to C.M.T. (cthiele@thielelab.de)

21

Extended Data Figure 1: **Synthesis of P*p*FABLA (1).** Reagents and conditions: (i) hydrazine monohydrate, triethylene glycol, 150 °C, 2 h, 46 % (ii) sodium nitrite, aqueous tetrafluoroboric acid solution, 0 °C, 1 h, 51 % (iii) *n*-butyllithium, tetrahydrofuran, −78 °C, 2 h, 84 % (iv) N-bromosuccinimide, TCE, 150 °C, 16 h, 64 % (v) N,N,N',N'-tetramethylguanidine, dimethylformamide / water, 40 °C, 3 d, 56 % (vi) phosgene, tetrahydrofuran, 20 °C, 2.5 h, 57 % (vii) dimethylethanolamine, dichloromethane, 20 °C, 16 d, 96 %.
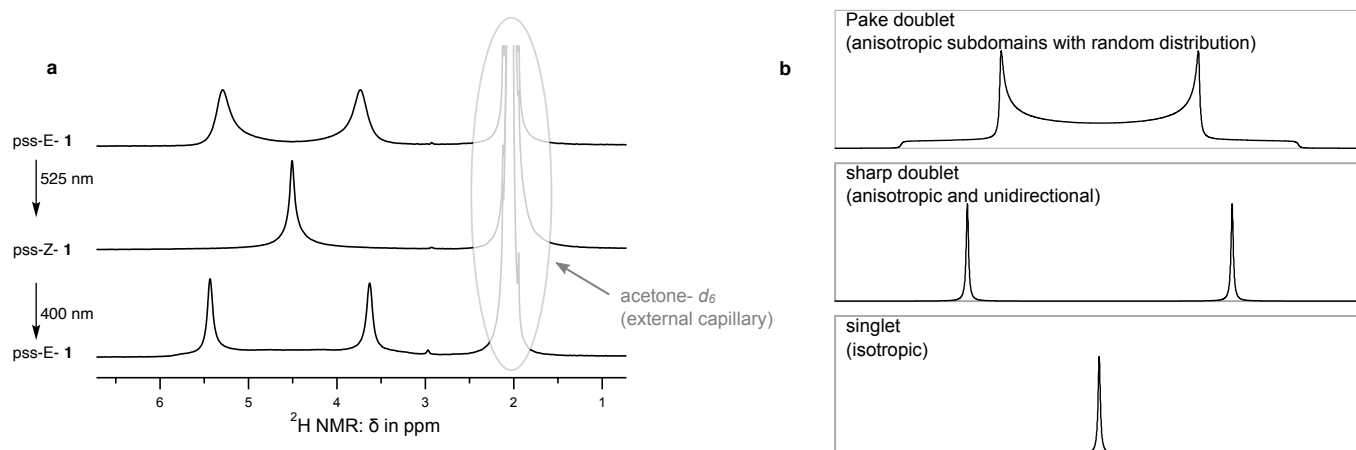
Extended Data Figure 2: **Photochromism of P*p*FABLA-*co*-PBLA (11). a**, Reversible photo-isomerisation of P*p*FABLA-*co*-PBLA (**11**), induced by green (525 nm) and violet (400 nm) light, respectively. **b**, UV-vis spectra of both pss (pss-E-**11**, solid line and pss-Z-**11**, dashed line) demonstrate a bathochromic shift of the azobenzene n-π* absorbance (> 380 nm) for E-**11** compared to Z-**11**. **c**, CD spectra reveal a left-handed helical secondary structure of both pss (positive CD of the backbone amide n-π* absorbance, 222 nm).
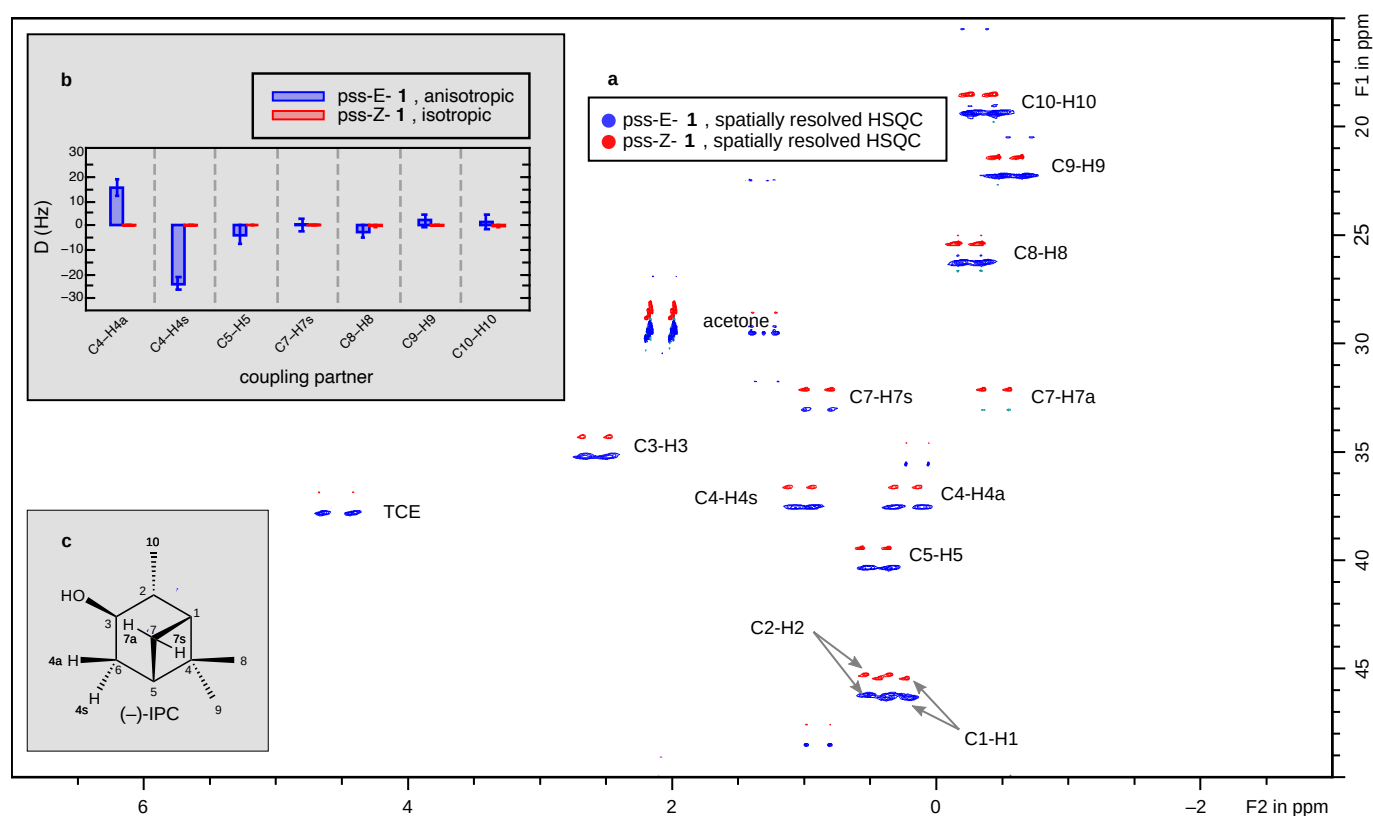
Extended Data Figure 3: **Monitoring photochromism of P*p*FABLA-*co*-PBLA (11)**. **a**, ^{19}F NMR spectra of P*p*FABLA-*co*-PBLA (**11**), acquired at 69.0, 100.0 and 175.5 min (pss-E-**11**, mixed state and pss-Z-**11**, respectively). **b**, Fraction of integrals a (Z-isomer, dashed line) and c (E-isomer, solid line) plotted vs. time obtained by *in-situ* irradiation NMR experiments with violet (400 nm) and green (525 nm) light for 70 and 110 min, respectively. **c**, Similar plot obtained in the absence of irradiation at 20 °C demonstrating the thermal stability of Z-**11**.

Extended Data Figure 4: **Quantification of *in-situ* irradiation ¹⁹F NMR polymer spectra.** If the azobenzenes in the side-chain are considered to be isolated from the polymer backbone, four ¹⁹F NMR signals (each belonging to two isochronous fluorines per residue of either the E-isomer or the Z-isomer) are expected. However, as the side-chains are not isolated from the backbone, more than four signals of the azobenzenes are possible[31]. Two signal sets (total of eight signals) result due to the influence of the secondary structure being helical and random-coil, respectively. The number of signal sets could be even higher, if the surroundings of the side-chain (e.g. the isomeric state of neighbouring azobenzenes) is taken into account. However, the latter influence (surroundings of the side-chain) on the chemical shift is presumably too small to be resolved (but contributes to broadened signals observed) and, thus, is not considered to increase the amount of expected ¹⁹F NMR signals. **a**, For P*p*FABLA (**1**), eight ¹⁹F NMR signals are expected but could not be resolved due to signal overlap. Therefore, only rough estimates of E/Z ratios are obtainable. **b**, For P*p*FABLA-*co*-PBLA (**11**), four ¹⁹F NMR signals are expected. In this case, only two signals overlap (region b, E- and Z-isomer) while regions a and c refer to signals of the Z-isomer and the E-isomer, respectively. Consequently, the sum of integrals a and c equalling integral b is a prerequisite for quantitatively interpretable spectra, which is met for P*p*FABLA-*co*-PBLA (**11**). Therefore, the spectra can be used for quantitative determination of E/Z ratios.

Extended Data Figure 5: **Reversible lyotropic liquid crystallinity**. A sample of 20 %(w/w) PpFABLA (**1**) dissolved in TCE-d_2 (identical to sample of Figure 3). **a**, ^{2}H NMR spectra of the solvent of the freshly prepared pss-E-**1** sample (top) after irradiation with green light resulting in pss-Z-**1** (middle) and with violet light resulting in pss-E-**1** (bottom). **b**, Expected ^{2}H NMR signal shapes for the solvent in anisotropic environment with randomly distributed subdomains (top, Pake doublet[34]), in anisotropic environment with unidirectional orientation (middle, sharp doublet) and in isotropic environment (bottom, singlet). The spectra were simulated using the software SIMPSON.[51]

Extended Data Figure 6: **Spatially resolved NMR spectra.** A sample of 20 %(w/w) P*p*FABLA (**1**) and (−)-IPC dissolved in TCE-*d₂*. The previously homogeneous pss-E-**1** sample has been irradiated locally with green light resulting in the lower part to be in pss-Z-**1** while the upper part remains in pss-E-**1** (identical to sample of Figure 3). **a**, Spatially resolved HSQC NMR spectra of the upper, anisotropic part (blue) and lower, isotropic part (red, shifted in the F1 dimension to enhance visibility) of the sample (slice width of 0.5 cm and spatial offset of 0.5 and −0.5 cm from the centre of the coil, respectively). **b**, Comparison of dipolar couplings extracted from both spectra. **c**, Structure of (−)-IPC.